Journal of Archaeological Science 50 (2014) 262–272

Contents lists available at ScienceDirect

Journal of Archaeological Science

journal homepage: http://www.elsevier.com/locate/jas

Combining image analysis and modular neural networks for classification of mineral inclusions and pores in archaeological potsherds

Anna Aprile [a, *], Giovanna Castellano [b], Giacomo Eramo [a]

[a] Department of Earth and Geoenvironmental Sciences, University of Bari "Aldo Moro", Via Orabona, 4, 70125 Bari, Italy
[b] Department of Computer Science, University of Bari "Aldo Moro", Via Orabona, 4, 70125 Bari, Italy

ARTICLE INFO

Article history:
Received 15 September 2013
Received in revised form
16 July 2014
Accepted 17 July 2014
Available online 29 July 2014

Keywords:
Image processing
Artificial neural network
Optical microscopy
Classification
Thin section
Archaeological pottery

ABSTRACT

The approach combining image analysis techniques and artificial neural networks is proposed here for automatic classification of mineral inclusions and pores in archaeological potsherds using optical digital images. Particularly, the automatic identification of quartz, calcareous aggregates and secondary porosity is considered. A collection of both plane and cross polarised light images acquired via a digital camera connected to optical microscopy in transmitted light is used. Images concern Holocene potsherds (8900–4200 years BP) from Takarkori rock shelter archaeological site (SW Libya, Central Sahara).

The adopted methodology involves different phases. Firstly, image segmentation is carried out to isolate regions corresponding to the interested mineral inclusions and pores. A segmentation procedure based on mathematical operators is customized for each type of inclusions and for pores. Secondly, numerical features are extracted from each segmented region, thus collecting data to perform automatic classification. A modular classifier is considered for classification, which is based on a combination of three two-layer feed-forward neural networks that are trained separately to recognise each class.

Experimental results show that the created modular classifier provides high classification accuracy for both inclusions and pores. The classifier was finally applied absent the image analysis phase on new samples to show the effectiveness of the proposed methodology.

1. Introduction

In ceramic petrography, optical polarising microscope is routinely used to study archaeological ceramics via observing thin sections of these materials. In this way, the *fabric*—as defined by the mineralogical composition, percentage, shape, size distribution and orientation of argillaceous minerals, non plastic inclusions and pores—can be characterised and classified. Thus, the definition of raw material sources and selection, forming techniques, chronology, decorative systems and firing conditions of ancient ceramics may be attained (Maggetti, 1982; Stoltman, 1989). However, drawbacks such as subjectivity and time-consuming of this practice should be overcome. Image analysis techniques gave an important contribution to such a purpose. Shape, size, roundness, etc. of minerals or grains may be actually automatically measured in this way and used to characterise rocks (Hofmann et al., 2011, 2013; Holden et al., 2009; Perring et al., 2004; Smith and Beermann, 2007) as well as archaeological ceramics and mortars, which can be actually considered as artificial rocks (Carò and Di Giulio, 2004; Casadio et al., 2005; Eramo et al., 2014; Livingood and Cordell, 2009; Middleton et al., 1985; Miriello and Crisci, 2006).

Recently, artificial neural networks (ANNs) coupled to image analysis used to perform automatic classification were considered also in optical mineralogy. In this approach, data extracted by image analysis relative to objects of interest are used as *features* for supervised training of ANNs. When presented with an unknown object, the network should have the ability to assign the object to its class, i.e. to finally classify that object.

Since some minerals share similar properties (particularly colour and brightness) depending on the interaction with light, image analysis based on optical digital images generally requires the assessment of ad-hoc hardware and processing algorithms to easily distinguish minerals during segmentation (Fueten and Goodchild, 2001; Herwegh, 2000; Soroushian et al., 2003; Wilson et al., 2007). However, although other image acquisition systems (e.g. digital X-ray maps by scanning electron microscopy) are also

* Corresponding author. Tel.: +39 0805442608.
E-mail addresses: annaaprile@libero.it, anna.aprile@uniba.it (A. Aprile), giovanna.castellano@uniba.it (G. Castellano), giacomo.eramo@uniba.it (G. Eramo).

http://dx.doi.org/10.1016/j.jas.2014.07.017
0305-4403/

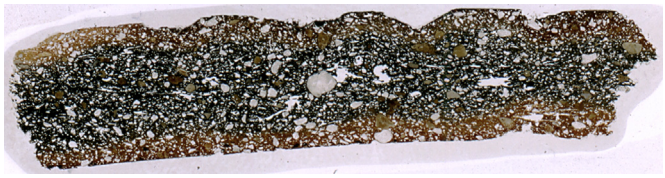

Fig. 1. Example of thin section belonging to QC fabric.

used (Knappett et al., 2011; Prêt et al., 2010), image analysis based on optical microscopy may provide a wide range of suitable features to automatically classify minerals and textures. Moreover, optical microscopy may be considered to be low-cost both for sample preparation and for the required hardware, especially if combined with the use of a freeware for image analysis.

Despite ANNs coupled to optical image analysis is used for automatic classification of minerals and textures of rocks (e.g. Baykan and Yilmaz, 2010; Fueten and Mason, 2007; Marmo et al., 2005; Singh et al., 2010; Thompson et al., 2001), to our knowledge this approach has not been applied till now to archaeological materials such as pottery. Actually, ANNs are used only at a macroscale for classification of potsherd decorations or as statistic method in chemiometric studies (Ma et al., 2000; Remolà et al., 1996; Stanco et al., 2011). However, as well as for rocks, the learning and generalization abilities of neural classifiers may be useful to "translate" heterogeneity of archaeological materials to attain their classification and characterisation.

Such an approach is thus proposed in this paper for archaeological pottery, specifically to face the problem of automatic identification of mineral inclusions and porosity. Particularly, quartz, calcareous aggregates and secondary porosity are considered.

The adopted methodology involved different phases. Digital plane and cross polarised light images were both acquired by thin sections. Image processing was then performed to segment regions corresponding to the interested inclusions and pores. Statistical and region features were hence extracted by each segmented region to be used for neural network training. Particularly, a modular architecture is used based on a combination of three neural networks each trained to recognise one class. The created modular neural classifier was finally applied absent the image analysis phase on new samples to evaluate its practical application for these types of mineral inclusions and for pores.

2. Materials

Some Holocene potsherds (8900–4200 BP) belonging to the Takarkori archaeological site (SW Libya, Central Sahara) are considered here as case study. A complete description of the archaeological context can be found in Eramo et al. (2014).

Petrographic observations distinguished three fabrics (named Q, QC and QF) for these potsherds according to different prevailing clastic constituents. The QC fabric is characterised by calcareous aggregates and quartz grains as mineral inclusions. The matrix presents high optical density due to carbonaceous matter, in some cases partially oxidised near the external surface and secondary pores related to the partial combustion of vegetal inclusions and organic matter, as well as to sintering occurred during firing. The QF fabric is rather characterised by potassium and plagioclase feldspars along with angular or sub-angular grains of quartz as mineral inclusions. The Q fabric has a very similar petrofacies compared to QC because characterised only by quartz inclusions. These two fabrics were already studied by using image analysis. Since of their mineralogical similarity, grain-size and morphometric data obtained in this way for quartz and calcareous aggregate inclusions were useful to determine the common fluviatile origin. Moreover, a compatibility with *wadi* and swamp sedimentary environments present in the area was found, which confirmed the local provenance of the raw materials (Eramo et al., 2014).

The 14 thin sections of potsherds belonging to fabric QC were used to assess the proposed methodology (Fig. 1).

3. Image analysis

The image analysis phase is devoted to create a set of labelled data to be used for the supervised learning of the ANNs. Particularly, in this phase, the knowledge about the interested classes, namely quartz, calcareous aggregates and pores, was used to segment images into the corresponding regions. After segmentation, feature extraction is performed so as to describe each region by a vector of numerical features. Precisely, a set of labelled samples (i.e. the segmented regions) for each class $c = 1 \ldots K$ (in our case $K = 3$) has to be created, each described by a feature-vector to be used for training the neural classifier.

To perform image analysis, four pairs of RGB digital images each composed by a plane and a cross polarised light image (denoted in the following respectively as P and XP) of 1920 × 2560 pixel size were acquired per thin section at a magnification of 2.5 × (1.315 μm/pixel) and then saved in TIFF format (Fig. 2). A ZEISS Axioskop 40 Pol petrographic microscope equipped with a Nikon DS-5MC digital camera with 2/3" CCD (Peltier cooling system) was used for acquisition. The four pairs of P and XP images were acquired by four different locations of each thin section, defined by maintaining a distance of 1 cm between the centre of each frame by the successive one and moving by one side to the other of the thin section.

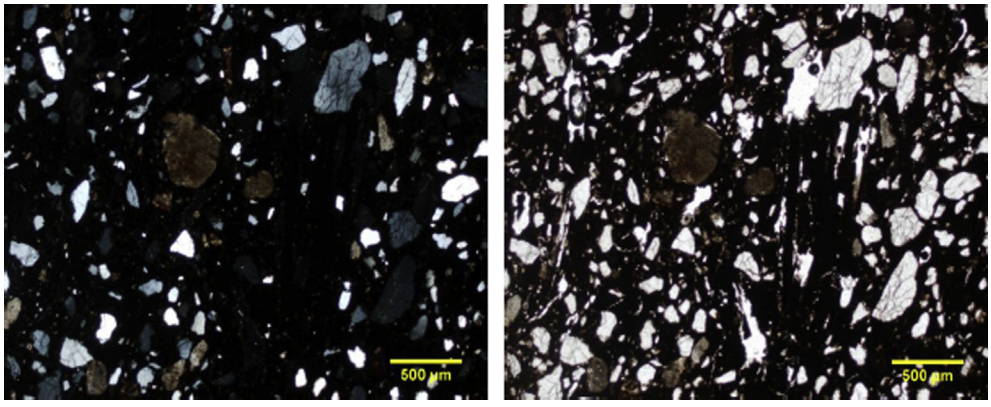

Fig. 2. Plane and cross polarised light digital images acquired by optical microscopy (example shown refers to sample named tk7).

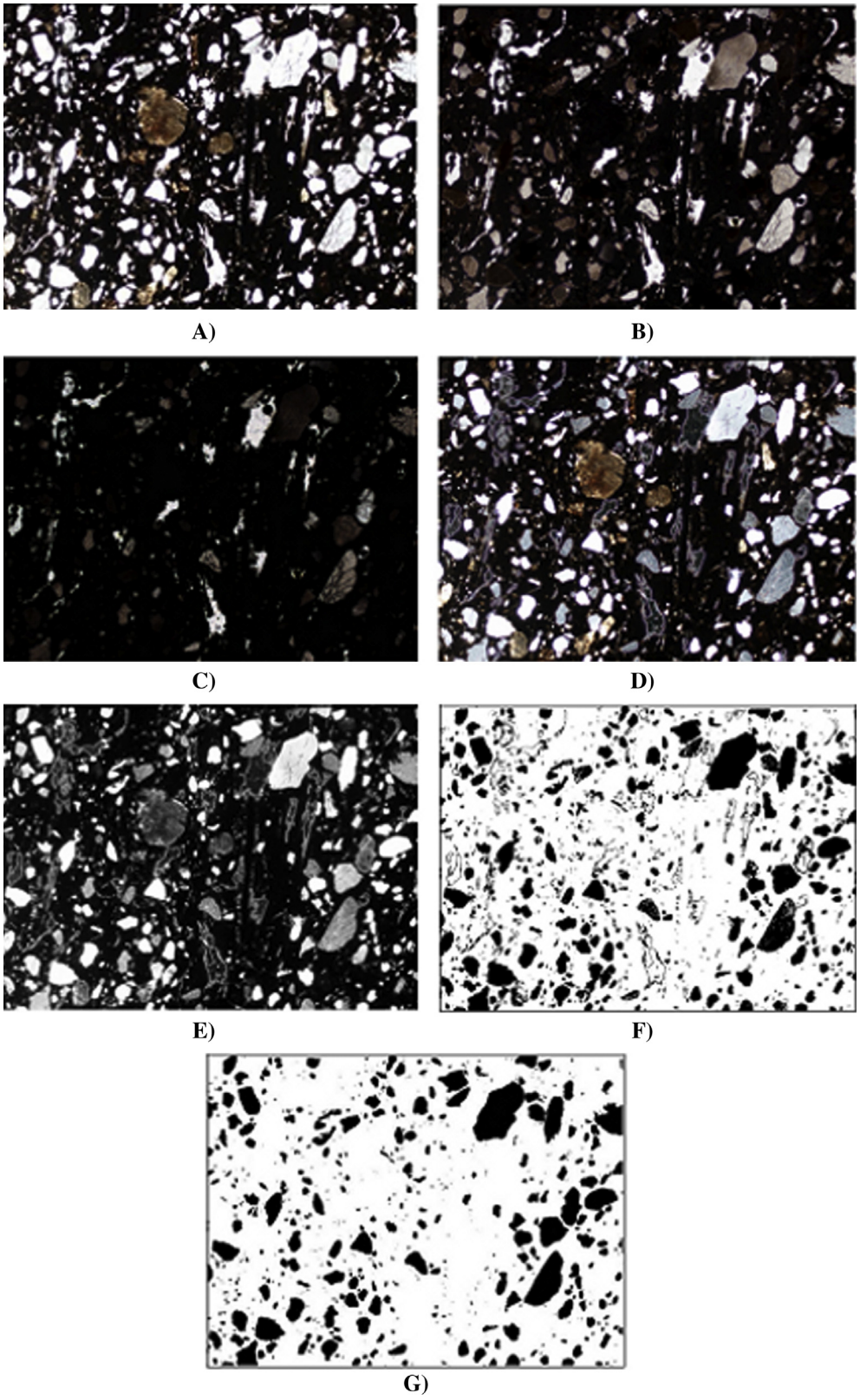

Fig. 3. Segmentation of quartz.

3.1. Segmentation

To segment regions corresponding to the three classes, both the acquired P and XP images were considered. The freeware open-source image analysis software *ImageJ* (version 1.42 and later; Rasband, 1997–2012) was used to such a purpose.

The manipulation of both kinds of images guarantees a better identification of minerals and the detection of characteristics useful

for segmentation. Particularly, as highlighted by Whitbread (1991), inclusion morphology is more clearly shown by the P images, while their mineralogical distinction is more easily achieved considering the interference colours revealed by the XP ones. The segmentation phase was primarily based on the use of mathematical operators to emphasize useful characteristics of the interested inclusions and pores. Then, the *Isodata* thresholding method (Ridler and Calvard, 1978) was finally applied. In this way, a customized segmentation procedure was developed for each class in order to derive corresponding targeted samples.

3.1.1. Segmentation of quartz

For segmentation of quartz, both P and XP images were manipulated together. Actually, some quartz grains are not visible using only XP images. At the same time, quartz grains are not easily distinguishable from pores if only P images are considered, since in these images the colours of pores (in the range of white values) are similar to the colours of quartz.

Particularly, P and XP images were firstly combined using the addition operator to obtain a new image where all the regions corresponding to quartz are morphologically well distinguishable and pixel brightness was minimized to have a better edge definition (Fig. 3A). However, the obtained image still showed the same range of colours for both quartz and pores. To avoid this effect, the XP image was subtracted by the P one using the subtraction operator (Fig. 3B). This procedure was inspired by the method proposed by Marinoni et al. (2005) for an experimental mortar thin section study via image analysis aimed to isolate porosity. Using this procedure, many quartz regions were distinguishable from pores since they were characterized by darker colours (grey-brownish areas of the image).

Lastly, to remove quartz regions that were still confused with pores, the exponential mathematical operator was applied to the previously obtained image, emphasizing high pixel values (Young et al., 1998) corresponding to pores (Fig. 3C). In this way, segmentation of quartz grains was obtained by progressively emphasizing the original range of colour values of pores.

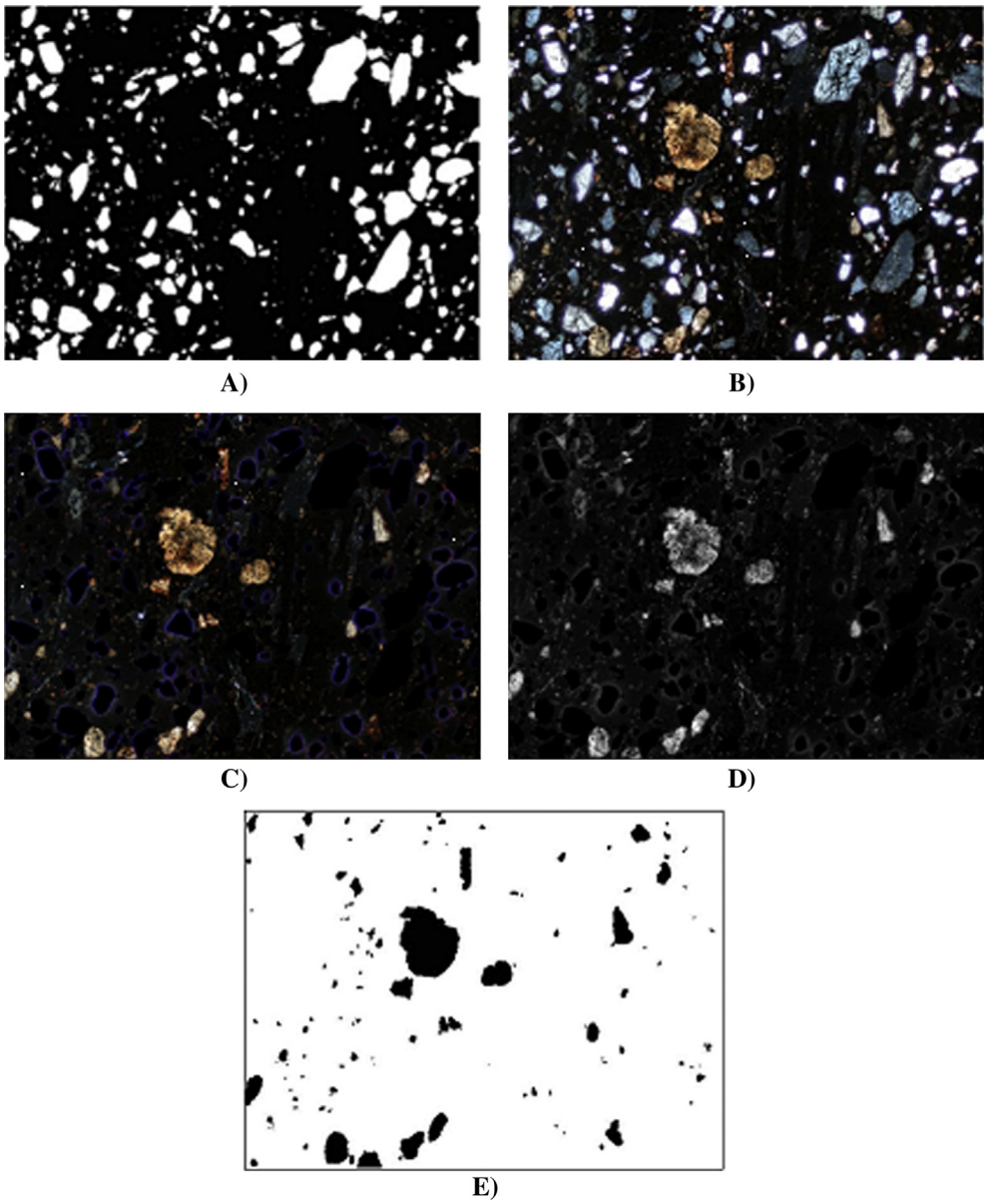

Fig. 4. Segmentation of calcareous aggregates.

Successively, the obtained image was subtracted by the image resulting by the addition operation in the first step in order to finally isolate quartz grains (Fig. 3D). Then, it was converted to 8-bit greyscale format (Fig. 3E) to be finally thresholded applying the *Isodata* method (Fig. 3F). The resulting binary map was then processed using the pixel eraser and the hole filling morphological operators to obtain the final binary image containing quartz regions (Fig. 3G).

3.1.2. Segmentation of calcareous aggregates

To segment calcareous aggregates, the differences in colours and texture with respect to quartz were considered. Actually, the calcareous aggregates show a sponge-like texture with less sharpen borders than quartz. Also, they show a colour range characterized by a prevalence of R (red) and G (green) combination (i.e. a particular light-to-dark brown colour). Moreover, a lower contrast was observed with respect to quartz. These differences are more clearly visible in XP images, therefore segmentation was performed using these images.

Firstly, the quartz binary image previously obtained (Fig. 3G) was inverted (i.e. the white colour was assigned to the inclusions) and filtered using the *Gaussian Blur*, the *Median* and the *Maximum* filters (Fig. 4A). These filters were used in order to guarantee a better overlap of the edges of grains in the binary image with respect to the corresponding ones in XP image and selected according to characteristics of each processed image. The filters were parameterized according to the default setting of the software, namely sigma = 2.0 for the Gauss filter and radius = 2.0 for the Median and the Maximum filters.

Next, the CLAHE (Contrast Limited Adaptive Histogram Equalization) method (Zuiderveld, 1994) was used for contrast enhancement of XP image to better distinguish calcareous aggregates from quartz (Fig. 4B). The quartz binary image initially inverted and filtered was then subtracted by corresponding XP image previously enhanced (Fig. 4C). The resulting image was finally converted in the 8-bit greyscale format (Fig. 4D) and then thresholded to produce the binary image of calcareous aggregates (Fig. 4E).

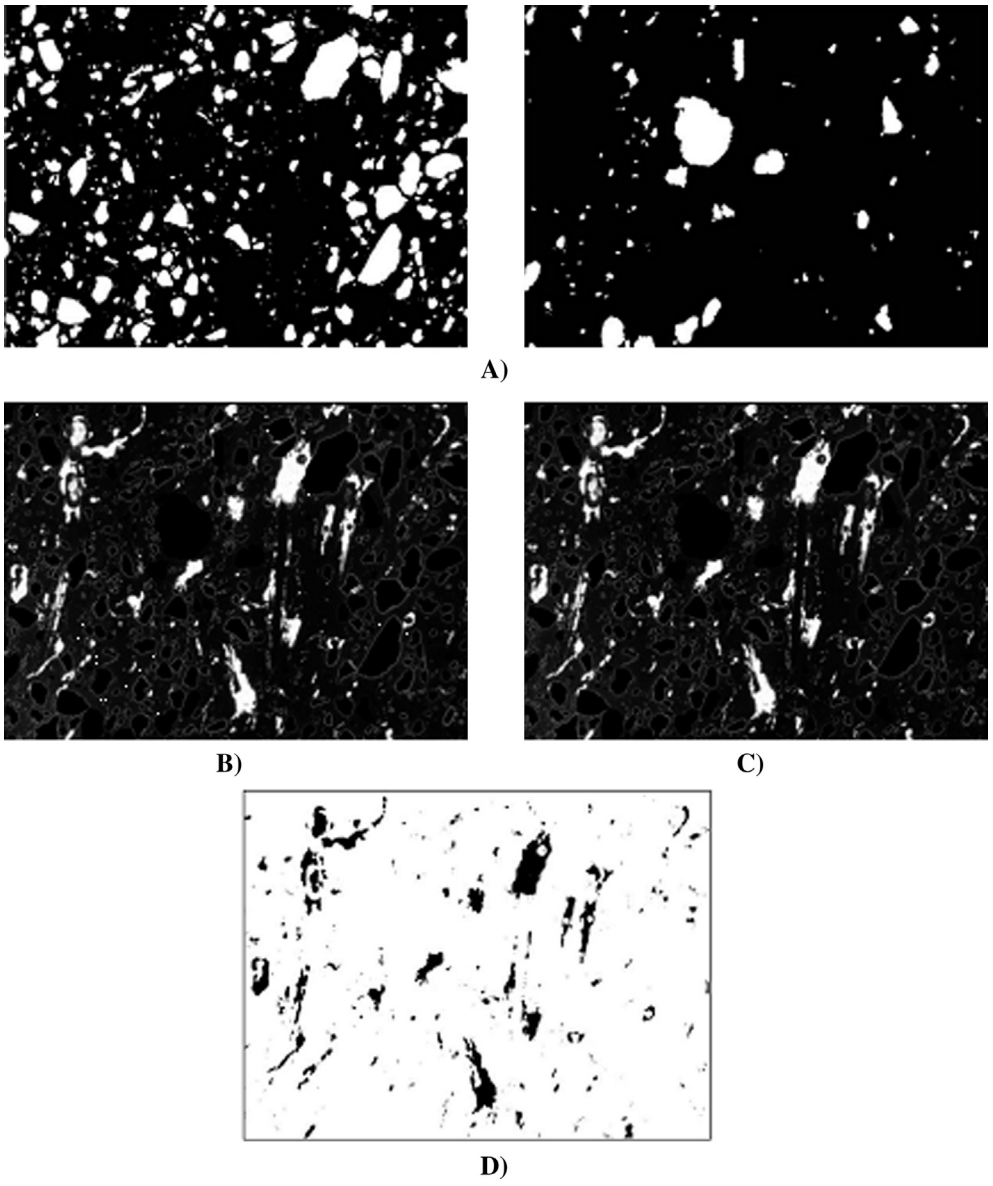

Fig. 5. Segmentation of pores.

3.1.3. Segmentation of pores

For the segmentation of pores, only P images were considered because they more clearly show morphology and colours of pores. Firstly, both the quartz and the calcareous aggregate binary images (Figs. 3G and 4E) were inverted and filtered using the same filters previously cited to guarantee a better overlap with the P image in the next steps (Fig. 5A). Then, each image was subtracted by the P image. The obtained image (Fig. 5B) was thus converted in the 8-bit greyscale format (Fig. 5C). The binary image showing pore regions was produced after thresholding and application of the median filter *Despeckle* (Fig. 5D) implemented in *ImageJ* to reduce noise, which exactly replaces each pixel value with the fifth median value in its 3×3 neighbourhood (Ferreira and Rasband, 2010–2012).

3.2. Feature extraction

To evaluate characteristics of inclusions and pores (i.e. colours, shape, orientation, etc.) and thus to accomplish the classification task, the neural classifier requires numerical features describing quantitatively these characteristics. As in other similar works (Baykan and Yilmaz, 2010; Singh et al., 2010), *statistical* and *region features* were considered here. Such features were computed by using the *ImageJ* plug-in *Particles8_Plus* (Landini, 2008).

Statistical features are descriptors of intensity histogram of the image or of the considered segmented regions related to moments of distribution and standard statistics of colours or grey tones (Gonzalez and Woods, 2002; Press et al., 1992). About region features, these parameters may be defined considering the *external descriptors* proposed by Gonzalez and Woods (2002) for regions in an image. However, different denominations are reported here according to the ones used by the adopted plug-in.

We extracted features by each singular region of quartz, calcareous aggregate and pore as obtained by segmentation, which refer to the corresponding areas of P and XP images. Particularly, the statistical features were computed for each R (red), G (green) and B (blue) colour channel related to the distribution histogram of the corresponding images. A 39 feature-vector for each region was thus provided to perform automatic classification. The extracted features are reported and briefly described in Table 1.

Table 1
Features used in this study.

Statistical features	Definition	Region features	Definition
Mode	Most occurring pixel value	Solidity	Area/convex area
Median	Median pixel value	Concavity	Convex hull-area
Average	Mean pixel value	Rectangularity	Area/area bounding box
Variance	Mean square deviation of pixel values from average		
Standard deviation	Standard deviation of pixel values		
Skewness	Degree of asymmetry of pixel value distribution		
Kurtosis	Peakedness of pixel value distribution		
Average deviation	Spread of pixel values from average		
Integrated density	Sum of pixel values		
Min	Minimum pixel value		
Max	Maximum pixel value		
Entropy	Degree of variability of pixel values		

4. The modular neural classifier

To distinguish among quartz, calcareous aggregates and pores, a modular architecture where each classifier is trained to classify one of the interested classes (Jacobs and Jordan, 1993; Sarkar, 2000) was adopted here. In this architecture, the classification problem is decomposed into a number of sub-problems addressed by modules that operate simultaneously on the same inputs without communicating each other. A combining scheme recombines the outputs of the modules to provide the final classification. The use of a modular classifier can help to improve the classification accuracy having the advantages of quick convergence, parallel training and better treatment of uncertainties (Briem et al., 2002; Sarkar, 2000).

Although different classification methods can be used to solve each sub-problem, the use of ANNs for each module was preferred here. ANNs are computational modelling tools that emulate the biological (human or animal) central nervous system in performing a particular task. An ANN is structured as a densely interconnected system of "artificial neurons", i.e. simple processing elements, forming input, hidden and output layers capable of acquisition, parallel data computation and knowledge representation (Bishop, 1996). ANNs are particularly suited in pattern classification or object recognition problems and when no algorithm or model is available to solve a problem; rather a large amount of data are available as examples to be used for supervised learning.

In the following, the neural network model used to implement the neural modules and the scheme for combining their outputs are described.

4.1. Creation of modules

As diffusely used for pattern recognition problems (Arel, 2012; Carson et al., 1995; Güler and Übeyli, 2005; Yildirim et al., 2004), a Multilayer Perceptron Neural Network (MLPNN) model was adopted here to implement each module. It is a feed-forward network generally consisting of an input layer with neurons representing input variables describing the problem, an output layer whose neurons correspond to variables describing what is being learnt and one or more hidden layers having neurons capable to capture the non linearity of the data. The set of outputs signals in the output layer constitutes the response of the network to the pattern provided as input (Bishop, 1996; Haykin, 1999).

Particularly, in this work a two-layer MLPNN with 39 inputs was used. One output is expected in the output layer since each module is created to classify one of the considered classes (Fig. 6).

The number of neurons in the hidden layer was ranged from 5 to 80 using a rate of 5 neurons. In this way, a total amount of 16 different two-layer MLPNN topologies were trained for each class. The MatLab® NPRTool (Neural Network Pattern Recognition Tool) v.7.10.0 (R2010a) was used to such a purpose.

To create the modules, the original three-class classification problem was primarily divided into three two-class problems following the *one-vs-rest* task decomposition scheme (Anand et al., 1995; Chen and You, 1993). According to this scheme, each neural module is used to discriminate patterns belonging to one class from patterns belonging to the remaining classes. Therefore, the *i-th* module or classifier is trained by using all patterns of class c as *positive samples* $\mathbf{T}_c^+$ and the remaining patterns as *negative samples* $\mathbf{T}_c^-$. The training set for each of the two-class problems was theoretically defined by

$$\mathbf{T}_c = \{\mathbf{x}_i, y_{ic}\}_{i=1}^{N_c} \quad \text{for c} = 1 \ldots K$$

where N_c is the number of training data, K is the number of classes (here $K = 3$), $\mathbf{x}_i$ is the input vector of the i-th training sample and y_{ic} is the desired output for the i-th training sample which is defined as

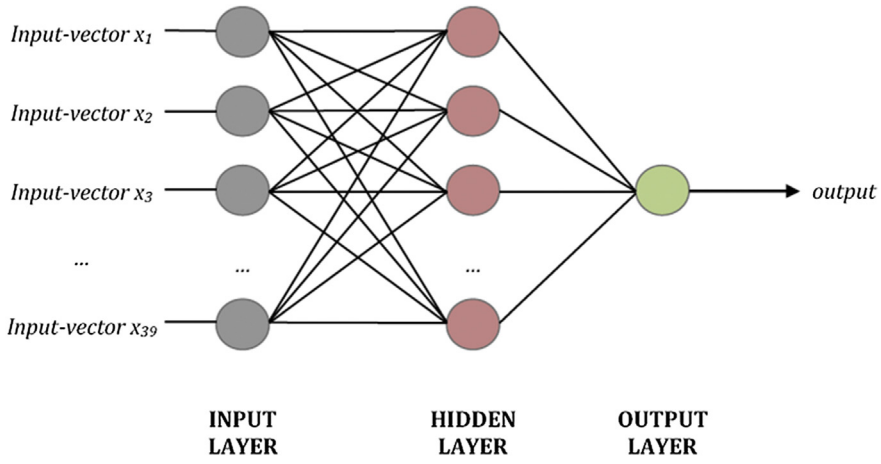

Fig. 6. The two-layer MLPNN network used in this study.

$$y_{ic} = \begin{cases} 1 & \text{if } \mathbf{x}_i \text{ belongs to class } c \\ 0 & \text{otherwise} \end{cases}$$

Particularly, the subset of positive samples for class c is $\mathbf{T}_c^+ = \{\mathbf{x}_i, y_{ic}\}_{i=1}^{N_c^+}$ where N_k^+ is the number of samples representative of class c, $\mathbf{x}_i$ is the feature-vector of the i-th sample and y_{ic} is the desired output for the i-th sample which is defined as $y_{ic} = 1$. The subset of negative samples for class c, uniformly taken from the sets $\mathbf{T}_k^+$, with $k \neq c$, is denoted as $\mathbf{T}_c^- = \{\mathbf{x}_i, y_{ic}\}_{i=1}^{N_c^-}$ where N_k^- is the number of samples that do not represent class c, $\mathbf{x}_i$ is yet the feature-vector of the i-th sample and y_{ic} is the desired output for the i-th sample which is defined as $y_{ic} = 0$. Precisely, to create a neural module capable of recognising each class c, the creation of a dataset $\mathbf{T}_c = \mathbf{T}_c^+ \cup \mathbf{T}_c^- = \{\mathbf{x}_i, y_{ic}\}_{i=1}^{N}$ is needed, where $N = N_k^+ + N_k^-$ is the total number of samples.

Given the training set T_c, a binary classifier has to be created which is capable to classify each input pattern in the correct class, i.e. to discriminate one class from the remaining two classes.

To perform training, each dataset was randomly split here into a 70% training set, a 15% test set and a 15% validation set. A supervised learning scheme called scaled conjugated backpropagation algorithm was adopted (Moller, 1993). Training was stopped when the minimum error on the validation set was reached[1] or when a maximum of 1000 epochs was achieved. To achieve more reliable results, 10 training runs were performed for each of the 16 network topologies starting from a different initial configuration of weights.

The classification error on the test set, defined as the probability of error in classifying new objects (Wanas et al., 1999), was considered to evaluate the classification accuracy of the trained networks. Precisely, the classification accuracy is calculated as the number of correctly classified samples over the total number of the considered ones, that is the sum of the true positive samples and the true negative samples over the total number of the considered ones (Fawcett, 2006).

To select the optimal neural network topology to be used as neural module in the modular architecture for each class, two different criteria were investigated. According to the former, the network topology providing the lowest classification error on the test set among the 160 trained networks was selected. According to the latter, the network topology providing the lower mean value of the classification error on the test set computed on the corresponding 10 training runs was primarily considered. Then, the configuration which returned the lower classification error among the 10 training run recorded for that topology was finally chosen.

[1] The training error generally decreases as training progresses while the validation set error only decreases up to a certain point after which it increases and this generally happens when an over-fitting of the data is reached by the network.

4.2. Recombination of modules

After each of the two-class problems was learnt by a MLPNN module, an output $f_c(\mathbf{x}_i)$ of the c-th classifier for input pattern $\mathbf{x}_i$ is returned and a function f_c is created so as to discriminate the patterns of class $c = 1 \ldots K$ (with $K = 3$) from those of the other classes. We created the modular classifier by applying simultaneously the three neural modules to an input pattern or assessment dataset and by combining their outputs in order to derive the final classification.

Several combination schemes for modular classifiers have been proposed in the literature (Lu and Ito, 1999; Sarkar, 2000). Particularly, we applied a standard recombination scheme based on the *winner-take-all* strategy, that works as follows. We denote by $f(\mathbf{x})$ the actual output vector of the modular classifier for the three-class classification problem. It can be written as

$$f(\mathbf{x}) = [f_1(\mathbf{x}), f_2(\mathbf{x}), f_3(\mathbf{x})]^T$$

Since the outputs $f_c(\mathbf{x}_i)$ returned by each classifier can be also interpreted as confidence values, a possible output value of 0.9, for example, means that a pattern is assigned to the positive class with a high confidence while a possible value of 0.3, on the other hand, means that the pattern should be considered negative with reservations. Namely, the larger the value, the more confidently the point $\mathbf{x}_i$ belongs to the class c. Thus, given an unknown input pattern $\mathbf{x}^*$, the combining scheme takes as final class the class with the highest confidence value. Precisely, the modular classifier assigns $\mathbf{x}^*$ to class c if the following condition holds:

$$|f_c(\mathbf{x}^*) - 1| \leq \delta \text{ and } |f_k(\mathbf{x}^*)| < \delta \quad \text{for } k \neq c \tag{1}$$

where δ is a real number, which denotes the error tolerance (in this work δ is set to 0.5).

For example, $f(\mathbf{x}^*) = [0.9, 0.4, 0.1]$ means that pattern $\mathbf{x}^*$ belongs to quartz, $f(\mathbf{x}^*) = [0.3, 0.7, 0.2]$ means that pattern $\mathbf{x}^*$ belongs to calcareous aggregates and $f(\mathbf{x}^*) = [0.3, 0.3, 0.8]$ means that pattern $\mathbf{x}^*$ belongs to pores (Fig. 7).

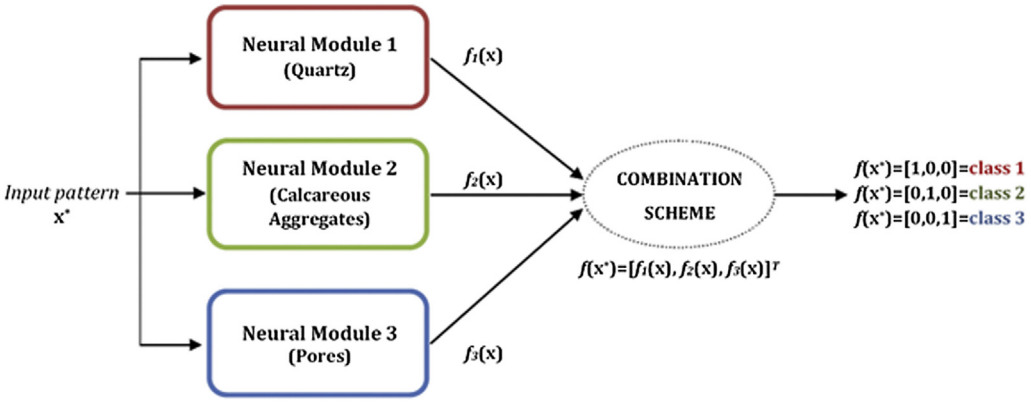

Fig. 7. Modular architecture adopted for classification.

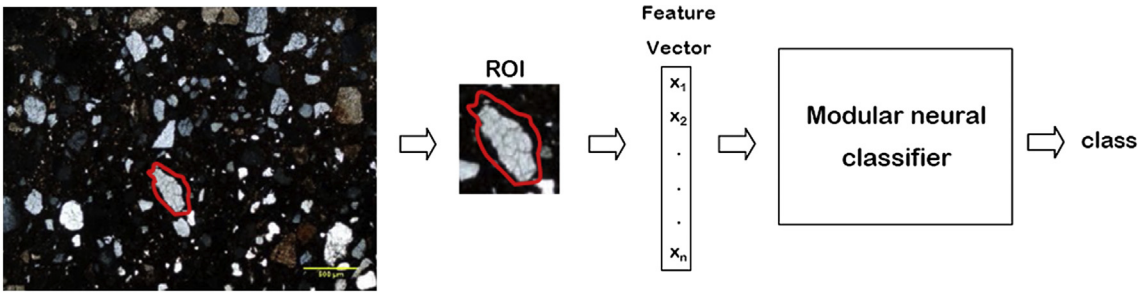

Fig. 8. Application of the created modular neural classifier absent the image analysis phase.

When condition (1) is not satisfied, the classification of $\mathbf{x}^*$ is considered ambiguous. For example $f(\mathbf{x}^*) = [0.8, 0.9, 0.2]$ means that $\mathbf{x}^*$ is recognised as belonging to both quartz and calcareous aggregates. In this case, the class of $\mathbf{x}^*$ is decided based on the *winner-take-all* strategy namely the pattern $\mathbf{x}^*$ is assigned to class c where $f_c(\mathbf{x}^*) = \max_{k=1\ldots K} f_k(\mathbf{x}^*)$, i.e. the class with the highest response.

Once properly assessed, the created modular classifier can be used to recognise the class of new samples absent the image analysis that did the initial classification. In this scenario, the user simply needs to manually select a ROI (i.e., region of interest) corresponding to any inclusion or pore he wants to know the class in an image of a new thin section of any potsherd and run the software that computes the 39 numerical features starting from that ROI. The corresponding feature-vector will be then used as input to the modular classifier, which will finally provide the class of that inclusion or pore. Fig. 8 illustrates this process.

5. Results

In this work, a total of 41,085 regions corresponding to quartz, 9313 regions corresponding to calcareous aggregates and 35,258 regions corresponding to pores were finally obtained by the adopted segmentation procedure (Section 3).

Then, in order to avoid the problem of unbalanced data for the three classes, the number of samples[2] to be used in the training set for each class was established by considering the number of available samples for the less abundant class (i.e. the calcareous aggregates). Thus, half of these samples as well as an equal number for the remaining classes were considered for training.

The remaining samples for each class were used to create an assessment dataset to test the modular classifier, which was finally composed by 3584 unknown samples, including respectively 1339 samples of quartz, 1089 of calcareous aggregates and 1156 of pores.

Classification errors on the test set provided by the trained networks for each of the three classes are shown in Fig. 9.

According to the first selection criterion (Section 4.1), the lowest error for class of quartz was achieved by a $39 \times 25 \times 1$ network, for calcareous aggregates by a $39 \times 5 \times 1$ network and for pores by a $39 \times 5 \times 1$ network (Table 2). These selected neural classifiers, combined into the modular classifier, finally achieved a classification accuracy of 90.1% when tested on the assessment dataset.

On the base of the second criterion, the lowest mean error was recorded for the $39 \times 45 \times 1$, the $39 \times 20 \times 1$ and the $39 \times 40 \times 1$ network topologies respectively for class of quartz, calcareous aggregates and pores, as shown in Table 3. The three selected classifiers were combined then to form a second modular classifier, that provided a classification accuracy of 89.8% on the same assessment dataset.

Since the two created modular classifiers provided similar classification accuracy, the accuracy-simplicity trade-off criterion was considered to finally select the best one. That is, the first modular classifier was actually chosen because it turns out to have a simpler topology (i.e., simpler network modules) than the second one.

As shown in the corresponding confusion matrix (Fig. 10), classification accuracy of the final modular classifier was higher for calcareous aggregates and quartz, while it was lower for pores. The quartz was mainly confused with the calcareous aggregates (70 errors over 76) as well as the calcareous aggregates and the pores were confused with the quartz (respectively 36 errors over 45 and 178 errors over 235).

[2] Recall that the term *sample* refers to each segmented region with its corresponding 39 feature-vector.

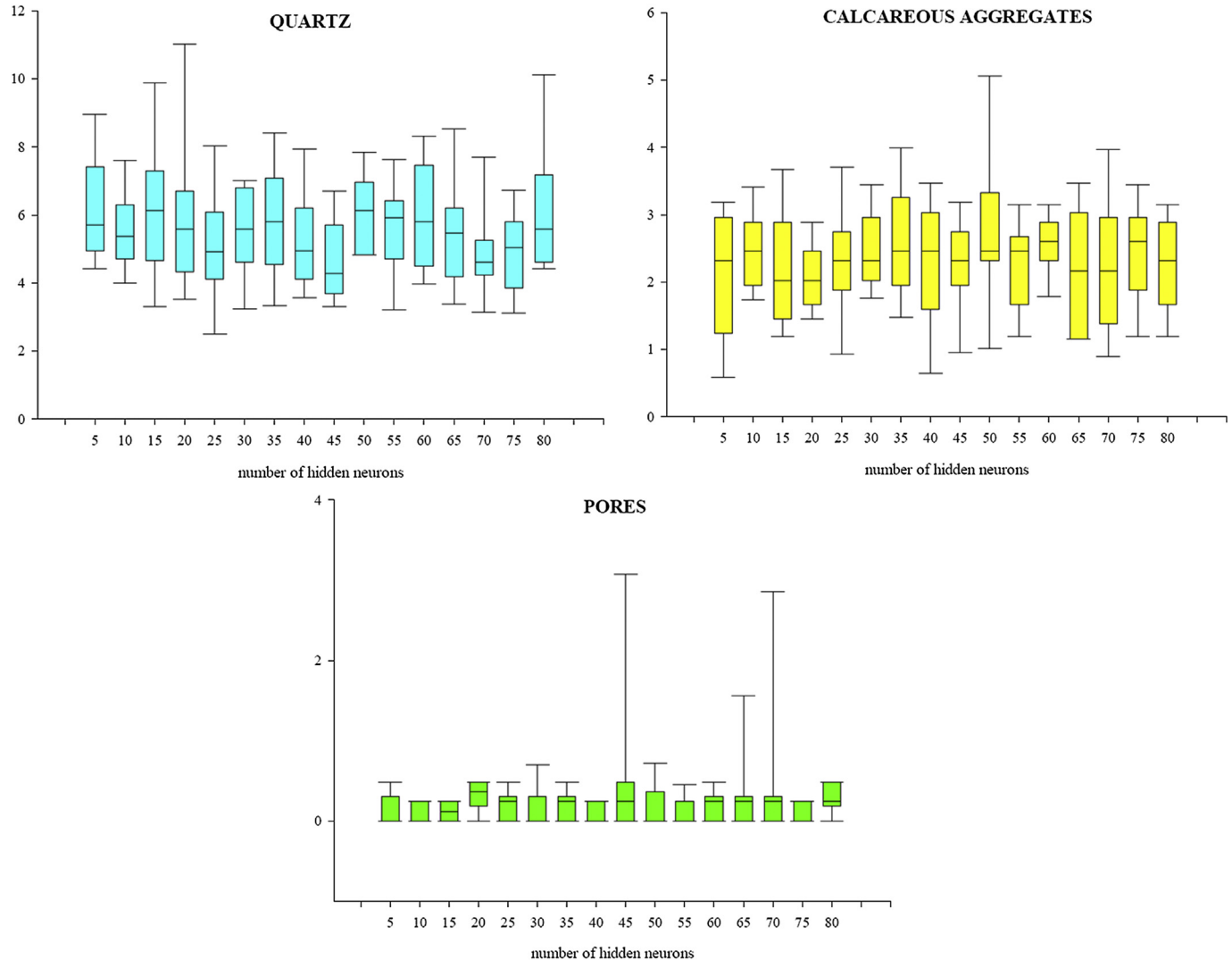

Fig. 9. Classification error on test set provided by the trained neural networks.

Table 2
Neural classifiers selected according to the first criterion.

Neural module	Topology	Classification error	Epochs
Quartz	39 × 25 × 1	2.41	76
Calcareous aggregates	39 × 5 × 1	0.58	58
Pore	39 × 5 × 1	0	77

Finally, Table 4 shows the results of classification as performed by the final modular classifier absent the image analysis phase on 9 new regions of inclusions and pores randomly selected by new images of potsherds. As confirmed by the expert, the modular classifier correctly classified all these new regions into the correct class.

Moreover, the final modular classifier was compared with a three-class monolithic classifier (namely capable to contemporarily

Table 3
Neural classifiers selected according to the second criterion.

Neural module	Topology	Classification error	Epochs
Quartz	39 × 45 × 1	3.29	85
Calcareous aggregates	39 × 20 × 1	1.45	53
Pore	39 × 40 × 1	0	31

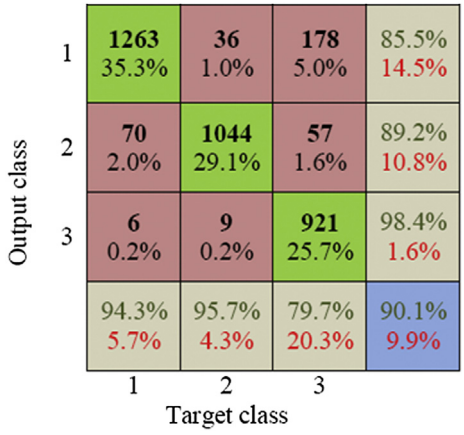

Fig. 10. Confusion matrix of modular classifier. A classification accuracy of 90.1% is reached by modular classifier on 3584 unknown samples, which is higher for calcareous aggregates and quartz (respectively 94.3% and 95.7%), while it is lower for pores (79.7%). Quartz is mainly confused with calcareous aggregates (70 errors over 76) as well as calcareous aggregates and pores are confused with quartz (respectively 36 errors over 45 and 178 errors over 235).

Table 4
Results of classification performed by the created modular classifier absent the image analysis phase. As confirmed by the expert, the modular classifier correctly classified all the new considered regions of inclusions and pores (ROI), randomly selected by new images of potsherds, into the correct class.

ROI	Class	ROI	Class	ROI	Class
	Pores	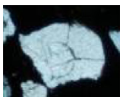	Quartz		Calcareous aggregates
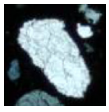	Quartz	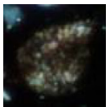	Calcareous aggregates		Pores
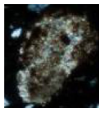	Calcareous aggregates	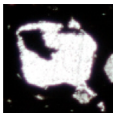	Pores	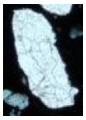	Quartz

distinguish among quartz, calcareous aggregates and pores) properly selected from several two-layer network topologies with 39 inputs and 3 outputs created using the same training conditions, which finally had a 39 × 10 × 3 topology. As it can be seen in Table 5, the modular classifier reached the better classification performance towards the monolithic network when tested on the same assessment dataset, except for quartz. Moreover, for both classifiers, the higher number of errors correspond to the class of pores, which has the lowest classification accuracy. The lower performance of the monolithic classifier is also shown by the number of epochs after which it converged to a solution (namely 106 epochs) which is higher than the ones of the classifiers composing the modular classifier shown in Table 2.

6. Discussion and conclusions

In this paper, a methodology for automatic classification of two types of mineral inclusions (i.e., quartz and calcareous aggregates) and of pores in archaeological potsherds is presented which combines image analysis and ANNs. Segmentation of inclusions and pores was performed using mathematical operators on both P and XP images. An automatic thresholding method was finally coupled to improve region detection. Then, rather than using a monolithic classifier, a modular architecture that combines as many neural classifiers as the number of classes was adopted for automatic classification.

At present, our preliminary results are encouraging and indicate that reliable features obtained by taking into account optical characteristics of the interested classes and a specific neural network architecture can provide a good automatic classification. Particularly, the better classification accuracy achieved for calcareous aggregates can be referred to their specific colours and texture (see Section 3.1.2) which probably led to the extraction of more distinctive features for this class. The confusion between quartz and calcareous aggregates may be referred to some samples of calcareous aggregates which appeared more light-blue coloured with respect to their common brownish colour, thus resembling typical quartz colouring. Meanwhile, the confusion between quartz and pores may be related to some samples of quartz which appeared lighter assuming similar colours as the pores. However, when tested absent the image analysis phase, the modular classifier assigned all the new samples to the correct class.

Moreover, the simulation results show that the classification accuracy of the proposed modular classifier is about the same as the corresponding monolithic one. However, while the classification performance of the modular classifier may be improved choosing other combinations of classifiers, the monolithic classifier topology remains fixed. This means that another classifier for the class of pore may be selected (also adopting other selection criteria) and combined into a new architecture, trying to reach better classification performance. Actually, the use of a modular classifier provides the possibility to grow up the original architecture with additional modules as soon as new classes were recognised and new data are available, with no need to re-creating the pre-existing modules. Moreover, each module can process data using different feature types and the most adequate classification technique according to the different case studies of natural and artificial rocks.

Further work will be devoted thus to the automatic classification of other mineral inclusions such as feldspars, micas, amphiboles and pyroxenes and to different kind of porosity, extending the modular classifier structure. Actually, the use of such an architecture may be considered particularly useful for the heterogeneous nature of archaeological materials.

This preliminary work represents a pilot study for the use of the proposed approach in ceramic petrography and a part of a more general methodological effort to classify pottery fabrics by ANNs. Future work must be then devoted to practical archaeometric application as well as temper analysis and recognition. Actually, a

Table 5
Classification accuracy of modular and monolithic classifier.

Class	Modular classifier				Monolithic classifier			
	Quartz	Calcareous aggregates	Pores	Total	Quartz	Calcareous aggregates	Pores	Total
Classification accuracy (%)	94.3	95.7	79.7	90.1	96.1	90.3	79.6	89.0
Number of errors	76	45	235	356	52	106	236	394

modular neural classifier may be used to distinguish temper addition from natural occurring inclusions, learning attributes characterizing the corresponding petrofacies or raw material sources. At higher level, we point to use modular classifiers to distinguish pottery fabrics via combination of compositional and morphometrical features of each component. In this way, modular architecture could be used to attribute each sample to a given fabric. For the considered case study, this could validate petrographic observations which initially led to distinguish the three fabrics as well as sedimentological interpretations highlighted by image analysis (Eramo et al., 2014).

References

Anand, R., Mehrotra, K.G., Mohan, C.K., Ranka, S., 1995. Efficient classification for multiclass problems using modular neural networks. IEEE Trans. Neural Netw. 6, 117–124.

Arel, E., 2012. Predicting the spatial distribution of soil profile in Adapazari/Turkey by artificial neural networks using CPT data. Comput. Geosci. 43, 90–100.

Baykan, N.A., Yilmaz, N., 2010. Mineral identification using color spaces and artificial neural networks. Comput. Geosci. 36 (1), 91–97.

Bishop, C.M., 1996. Neural Networks for Pattern Recognition. Oxford University Press Inc., Oxford, 504 pp.

Briem, G., Benediktsson, J.A., Sveinsson, J.R., 2002. Multiple classifiers applied to multisource remote sensing data. IEEE Trans. Geosci. Remote Sens. 40 (10), 2291–2299.

Carò, F., Di Giulio, A., 2004. Reliability of textural analysis of ancient plasters and mortars through automated image analysis. Mater. Charact. 53, 243–257.

Carson, C.A., Keller, J.M., McAdoo, K.K., Wang, D., Higgins, B., Bailey, C.W., Thorne, J.G., Payne, B.J., Skala, M., Hahn, A.W., 1995. Escherichia coli O157:H7 restriction pattern recognition by artificial neural network. J. Clin. Microbiol. 33, 2894–2898.

Casadio, F., Chiari, G., Simon, S., 2005. Evaluation of binder/aggregate ratios in archaeological lime mortars with carbonate aggregate: a comparative assessment of chemical, mechanical and microscopic approaches. Archaeometry 47 (4), 671–689.

Chen, C.H., You, G.H., 1993. Class-sensitive neural network. Neural Parallel Sci. Comput. 1 (1), 93–96.

Eramo, G., Aprile, A., Muntoni, I.M., Zerboni, A., 2014. Textural and morphometric analysis applied to Holocene pottery from Takarkori rock shelter (SW Libya, Central Sahara): a quantitative sedimentological approach. Archaeometry 56 (Suppl. 1), 36–57.

Fawcett, T., 2006. An introduction to ROC analysis. Pattern Recognit. Lett. 27, 861–874.

Ferreira, T., Rasband, W.S., 2010–2012. ImageJ User Guide – IJ 1.46. http://imagej.nih.gov/ij/docs/guide/.

Fueten, F., Goodchild, J.S., 2001. Quartz c-axes orientation determination using the rotating polarizer microscope. J. Struct. Geol. 23, 895–902.

Fueten, F., Mason, J., 2007. An artificial neural net assisted approach to editing edges in petrographic images collected with the rotating polarizer stage. Comput. Geosci. 33, 1176–1188.

Gonzalez, R.C., Woods, R.E., 2002. Digital Image Processing, second ed. Prentice Hall Inc., Upper Saddle River, New Jersey. 793 pp.

Güler, I., Übeyli, E.D., 2005. Detection of ophthalmic arterial doppler signals with Behcet disease using multilayer perceptron neural network. Eng. Appl. Artif. Intell. 35, 413–422.

Haykin, S., 1999. Neural Networks: a Comprehensive Foundation. Macmillan, New York, 823 pp.

Herwegh, M., 2000. A new technique to automatically quantify microstructures of fine grained carbonate mylonites: two-step etching combined with SEM imaging and image analysis. J. Struct. Geol. 22, 391–400.

Hofmann, P., Marschallinger, R., Unterwurzacher, M., Zobl, F., 2011. Designation of marble provenance: state-of-art rock fabric characterization in thin sections by object based image analysis. In: Marschallinger, R., Zobl, F. (Eds.), Proceedings IAMG 2011, pp. 1198–1211.

Hofmann, P., Marschallinger, R., Unterwurzacher, M., Zobl, F., 2013. Marble provenance designation with object based image analysis: state-of-the-art rock fabric characterization from petrographic micrographs. Austrian J. Earth Sci. 106/2, 40–49.

Holden, E.J., Moss, S., Russell, J.K., Dentith, M.C., 2009. An image analysis method to determine crystal size distributions of olivine in kimberlite. Comput. Geosci. 13, 255–268.

Jacobs, R.A., Jordan, M.I., 1993. Learning piecewise control strategies in a modular neural network architecture. IEEE Trans. Syst. Man Cybern. 23, 337–345.

Knappett, C., Pirrie, D., Power, M.R., Nikolakopoulou, I., Hilditch, J., Rollinson, G.K., 2011. Mineralogical analysis and provenancing of ancient ceramics using automated SEM-EDS analysis (QEMSCAN®): a pilot study on LB I pottery from Akrotiri, Thera. J. Archaeol. Sci. 38, 219–232.

Landini, G., 2008. Advanced shape analysis with ImageJ. In: Proceedings of the Second ImageJ User and Developer Conference, Luxembourg, 6–7 November, pp. 116–121. Plug-ins available from: http://www.mecourse.com/landinig/software/software.html.

Livingood, P.C., Cordell, A.S., 2009. Point/counter point: the accuracy and feasibility of digital image techniques in the analysis of ceramic thin sections. J. Archaeol. Sci. 36, 867–872.

Lu, B.-L., Ito, M., 1999. Task decomposition and module combination based on class relations: a modular neural network for pattern classification. IEEE Trans. Neural Netw. 10 (5), 1244–1256.

Ma, Q., Yan, A., Hu, Z., Li, Z., Fan, B., 2000. Principal component analysis and artificial neural networks applied to the classification of Chinese pottery of Neolithic age. Anal. Chim. Acta 406, 247–256.

Maggetti, M., 1982. Phase analysis and its significance for technology and origin. In: Olin, G.S., Franklin, A.D. (Eds.), Archeological Ceramics. Smithsonian Institution Press, Washington, pp. 121–133.

Marinoni, N., Pavese, A., Foia, M., Trombino, L., 2005. Characterisation of mortar morphology in thin sections by digital image processing. Cem. Concr. Res. 35, 1613–1619.

Marmo, R., Amodio, S., Tagliaferri, R., Ferreri, V., Longo, G., 2005. Textural identification of carbonate rocks by image processing and neural network: methodology proposal and examples. Comput. Geosci. 31, 649–659.

Middleton, A.P., Freestone, I.C., Leese, M.N., 1985. Textural analysis of ceramic thin sections: evaluation of grain sampling procedures. Archeometry 27 (1), 64–74.

Miriello, D., Crisci, G.M., 2006. Image analysis and flatbed scanners. A visual procedure in order to study the macro-porosity of the archaeological and historical mortars. J. Cult. Herit. 7, 186–192.

Moller, M.F., 1993. A scaled conjugate gradient algorithm for fast supervised learning. Neural Netw. 6, 525–533.

Perring, C.S., Barnes, S.J., Verrall, M., Hill, R.E.T., 2004. Using automated digital image analysis to provide quantitative petrographic data on olivine–phyric basalts. Comput. Geosci. 30, 183–195.

Press, W.H., Teukolsky, S.A., Vetterling, W.T., Flannery, B.P., 1992. Numerical Recipes in C, the Art of Scientific Computing. Cambridge University Press, Cambridge, UK, 610 pp.

Prêt, D., Sammartino, S., Beaufort, D., Meunier, A., Fialin, M., Michot, L.J., 2010. A new method for quantitative petrography based on image processing of chemical element maps: part I. Mineral mapping applied to compacted bentonites. Am. Mineral. 95, 1379–1388.

Rasband, W.S., 1997–2012. ImageJ. U.S. National Institutes of Health, Bethesda, Maryland, USA. http://imagej.nih.gov/ij/.

Remolà, J.A., Lozano, J., Ruisánchez, I., Larrechi, M.S., Rius, F.X., Zupan, J., 1996. New chemiometric tools to study the origin of amphorae produced in the Roman Empire. Trend Anal. Chem. 15 (3), 137–151.

Ridler, T.W., Calvard, S., 1978. Picture thresholding using an iterative selection method. IEEE Trans. Syst. Man Cybern. 8, 630–632.

Sarkar, M., 2000. Modular pattern classifiers: a brief survey. IEEE Int. Conf. Syst. Man Cybern. 4, 2878–2883.

Singh, N., Singh, T.N., Tiwary, A., Sarkar, K.M., 2010. Textural identification of basaltic rock mass using image processing and neural network. Comput. Geosci. 14, 301–310.

Smith, J.V., Beermann, E., 2007. Image analysis of plagioclase crystals in rock thin sections using grey level homogeneity recognition of discrete areas. Comput. Geosci. 33, 335–356.

Soroushian, P., Elzafraneya, M., Nossoni, A., 2003. Specimen preparation and image processing and analysis techniques for automated quantification of concrete microcracks and voids. Cem. Concr. Res. 33, 1949–1962.

Stanco, F., Tanasi, D., Guarnera, G.C., Gallo, G., 2011. Automatic classification of decorative patterns in the Minoan pottery of Kamares style. In: Papaodysseus, C. (Ed.), Pattern Recognition and Signal Processing in Archaeometry: Mathematical and Computational Solutions for Archaeology, pp. 186–211.

Stoltman, J.B., 1989. A quantitative approach to the petrographic analysis of ceramic thin sections. Am. Antiq. 54 (1), 147–160.

Thompson, S., Fueten, F., Bockus, D., 2001. Mineral identification using artificial neural networks and the rotating polarizer stage. Comput. Geosci. 27, 1081–1089.

Wanas, N., Kamel, M.S., Auda, G., Karray, F., 1999. Feature-based decision aggregation in modular neural network classifiers. Pattern Recognit. Lett. 20, 1353–1359.

Whitbread, I.K., 1991. Image and data processing in ceramic petrology. In: Middleton, A., Freestone, I. (Eds.), Recent Developments in Ceramic Petrology, pp. 369–386. London, British Museum Occasional Paper n.81.

Wilson, C.J.L., Russell-Head, D.S., Kunze, K., Viola, G., 2007. The analysis of quartz c-axis fabrics using a modified optical Microscope. J. Microsc. 227 (1), 30–41.

Yildirim, H., Haltinsoy, H.B., Barişçi, N., Ergün, U., Ogur, E., Hardalaç, F., Güler, I., 2004. Classification of the frequency of carotid stenosis with MLP and RFB neural networks in patients with coroner artery disease. J. Med. Syst. 28 (6), 591–601.

Young, I.T., Gerbrands, J.J., Van Vliet, L.J., 1998. Fundamentals of Image Processing. Delft University of Tecnology Eds., 113 pp.

Zuiderveld, K., 1994. Contrast limited adaptive histogram equalization. In: Heckbert, P. (Ed.), Graphics Gems IV. Academic Press Professional Inc., San Diego, pp. 474–485.